Supporting Information

MXene-Antenna Electrode with Collective Multipole Resonances

Vahid Karimi   Viktoriia E. Babicheva*

Department of Electrical and Computer Engineering, University of New Mexico,
Albuquerque, New Mexico 87131, USA
E-mail: vbb@unm.edu

Single antenna

We calculate the absorption, extinction, and scattering cross-section efficiencies using Mie theory for a single spherical antenna of MXene with diameter $2R$ placed in a uniform optical environment with the refractive index of unity $n = 1$ (**Figure S1**). The cross-section efficiencies are presented as colormap with varying wavelength λ (in vacuum) and antenna size. One can notice that ED and EQ resonances are considerably stronger than their magnetic counterparts. One can see in absorption cross-section efficiencies that ED and EQ resonances have maxima at radii of about 100-200 nm and 250-450 nm, respectively. In contrast, for magnetic dipole and quadrupole, the radius corresponding to the maximum is less than 200 nm.

Electric field distribution

Figure S2 shows electric field distribution around the antenna in two different cases.

Antenna shape

Figure S3 shows the response of arrays with various antenna shapes with equal periodicities $D_x = D_y$ = 1500 nm. Antenna dimensions for different shapes are similar to the parameters selected for the sphere array. One can see that for the current arrangement, the cuboids and disks with the characteristic size of ~700 nm have larger absorption than spheres. Details of the configurations for the full-wave numerical simulations are as follows: **a** spheres $2R = 900$ nm, **b** disks $2R = a_z = 700$ nm, **c** cubes $a_x = a_y = a_z = 700$ nm, **d** cuboids $(a_x = 600) \times (a_y = 700) \times (a_z = 700)$ nm^3, and **e** cuboids $(a_x = 700) \times (a_y = 600) \times (a_z = 700)$ nm^3.

Bridge width

Figure S4a and **b** show the numerical simulations of absorption spectra under the illumination with light with x- or y-polarization, respectively. Figure S4 displays resonant excitations in the interconnected MXene antennas arranged with periodicities $D_y = D_x = 1500$ nm as depicted in Figure 1**c** of the main text. We consider MXene antennas of cube shape with $a_x = a_y = a_z = 700$ nm connected with 'bridges' with the width w varying from 100 nm to 700 nm (in the increment of 100 nm) in the uniform surrounding with $n = 1$. As expected, absorption profiles gradually decrease as the bridge width gets wider, and the resonances vanish.

MXene permittivity and its variations

Figure S5a shows permittivity of Ti$_3$C$_2$T$_x$ MXene. **Figure S5b** and **c** show the simulation results for MXene spheres with $R = 450$ nm and arranged into an array with a periodicity of 1500 nm. The plots in the panels **b** and **c** are absorption under variation of the real and imaginary parts, respectively. We observe that such variations do not result in dramatic changes in the absorption profiles. The response of the sphere array is relatively uniform under variation of the imaginary part, while the variation of the real
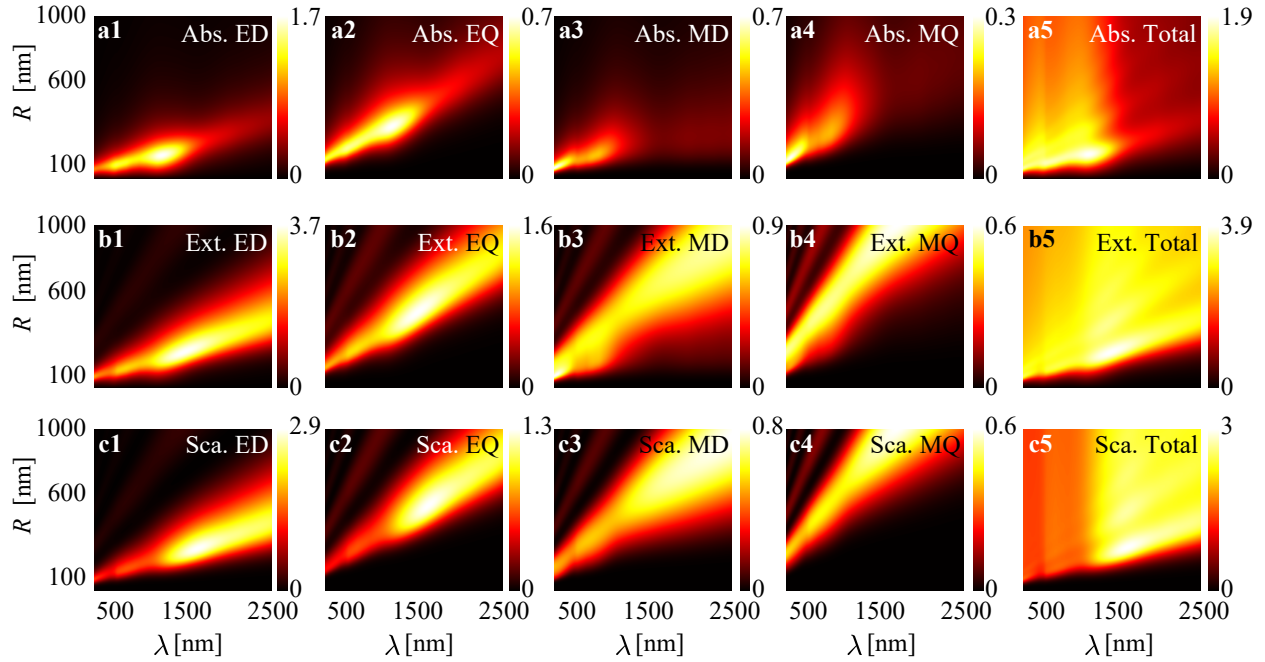
Figure S1: The cross-section efficiencies dependent on the incident wave with the wavelength λ in air and antenna size. Absorption, extinction, and scattering efficiencies are obtained using the Mie theory for a single sphere antenna of MXene with radius R located in a uniform dielectric environment with the refractive index $n = 1$. **a1-a5** Absorption efficiency, **b1-b5** Extinction efficiency, and **c1-c5** Scattering efficiency. Each set shows multipolar excitation and total cross-section efficiencies. Electric dipole and quadrupole are denoted as 'ED' and 'EQ', and magnetic dipole and quadrupole are denoted as 'MD' and 'MQ', respectively.
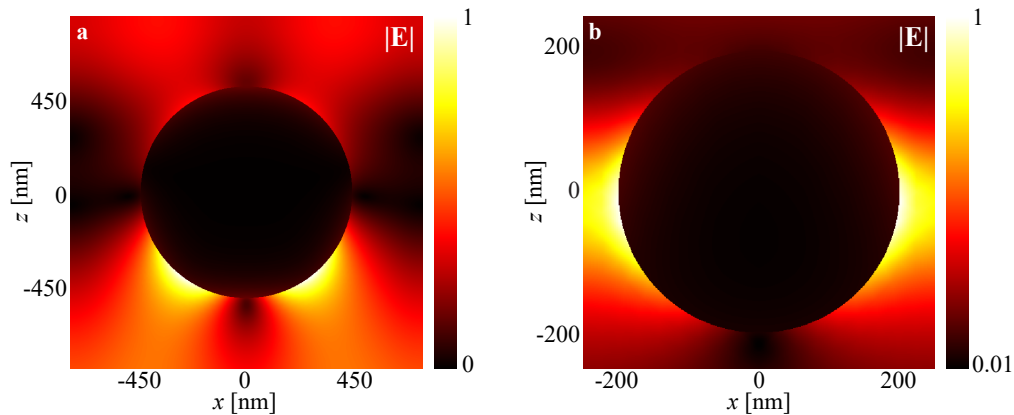

Figure S2: Normalized electric field distribution of the mode excited at $\lambda = 1500$ nm in the xz-cross-section at $y = 0$. **a** $R = 450$ nm, $D_y = 1500$ nm, and $D_x = 1500$ nm. **b** $R = 200$ nm, $D_y = 2300$ nm, and $D_x = 500$ nm. The set of parameters in panel **a** corresponds to the condition when both ED and EQ are excited approximately at the same wavelength. The electric field has a hybrid ED/EQ distribution. This excitation of ED and EQ results in a field distribution such that the backward scattering is suppressed, and we observe a generalized lattice Kerker effect in the reflection spectrum. Panel **b** corresponds to the ED excitation. In both cases, we see that the field is mostly localized on the surface of the antenna and outside of it.
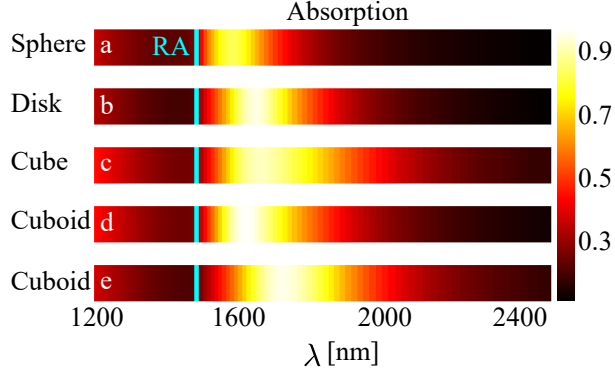
Figure S3: Excitation of resonances in the MXene antenna array of **a** spheres ($2R = 900$ nm), **b** disks ($2R = a_z = 700$ nm), **c** cubes ($a_x = a_y = a_z = 700$ nm), **d** cuboids (with the dimensions $(a_x = 600) \times (a_y = 700) \times (a_z = 700)$ nm^3) and **e** cuboids (with the dimensions $(a_x = 700) \times (a_y = 600) \times (a_z = 700)$ nm^3). The absorption profiles are obtained with the full-wave numerical simulations with $D_x = D_y = 1500$ nm. The solid cyan line denotes the Rayleigh anomaly wavelength: 'RA' denotes the Rayleigh anomaly.

part results in slight deviations. The interval of permittivity changes in panel **b** is twice of the interval in panel **c**.

Array schematic

Figure S6 shows the schematic of an array of antennas of $Ti_3C_2T_x$ MXene under perpendicular illumination of x-polarized plane wave.

Antenna polarizability

Figure S7 shows real and imaginary parts of ED and EQ effective polarizability of the antenna placed in the lattice. At the corresponding resonances, the effective polarizabilities of those two multipoles are calculated. In panel **a** for α_{ED}, the antenna radius is 200 nm, and the array periods are $D_x = 500$ nm and $D_y = 2300$ nm. In panels **b** and **c** for α_{ED} and α_{EQ}, respectively, the antenna radius is 450 nm and the array periods are $D_x = 1500$ nm and $D_y = 1200$ nm. In panel **a** near the Rayleigh anomaly wavelength, the MXene array with antennas of $R = 200$ nm shows similar conventional ED lattice resonance of plasmonic behavior. There, the real part of the antenna's effective polarizability changes its sign, and the imaginary part has a maximum. In panel **b**, for the radius of 200 nm, the effective polarizability of the ED lattice resonance shows an inverse nature to conventional resonances: at the Rayleigh anomaly wavelength, it has an unpronounced maximum of Re[α_{ED}] with no rapid change of Im[α_{ED}]. The reason is ED single-antenna polarizability is very small for the radius $R = 450$ nm, and the effective polarizability of the antennas in the array α_{ED} is mainly defined by the lattice sums. In panel **c**, a strong EQ resonance is observed. The maximum of Re[α_{EQ}] is offset from λ_{RA}, and we see the same offset for the extinction cross-section maximum as well. The maximum of Im[α_{EQ}] almost matches λ_{RA} and varies steeply. In panels **b** and **c**, polarizabilities of ED and EQ have no negative magnitude for the longer wavelength than the Rayleigh anomaly.

Repeatability of experimental measurements

We measure transmission through the antenna arrays that correspond to several additional samples (#1 through #8, **Figure S8**). Comparison to the results for the Sample #0 shown in the main text indicates a good agreement of the measurements.
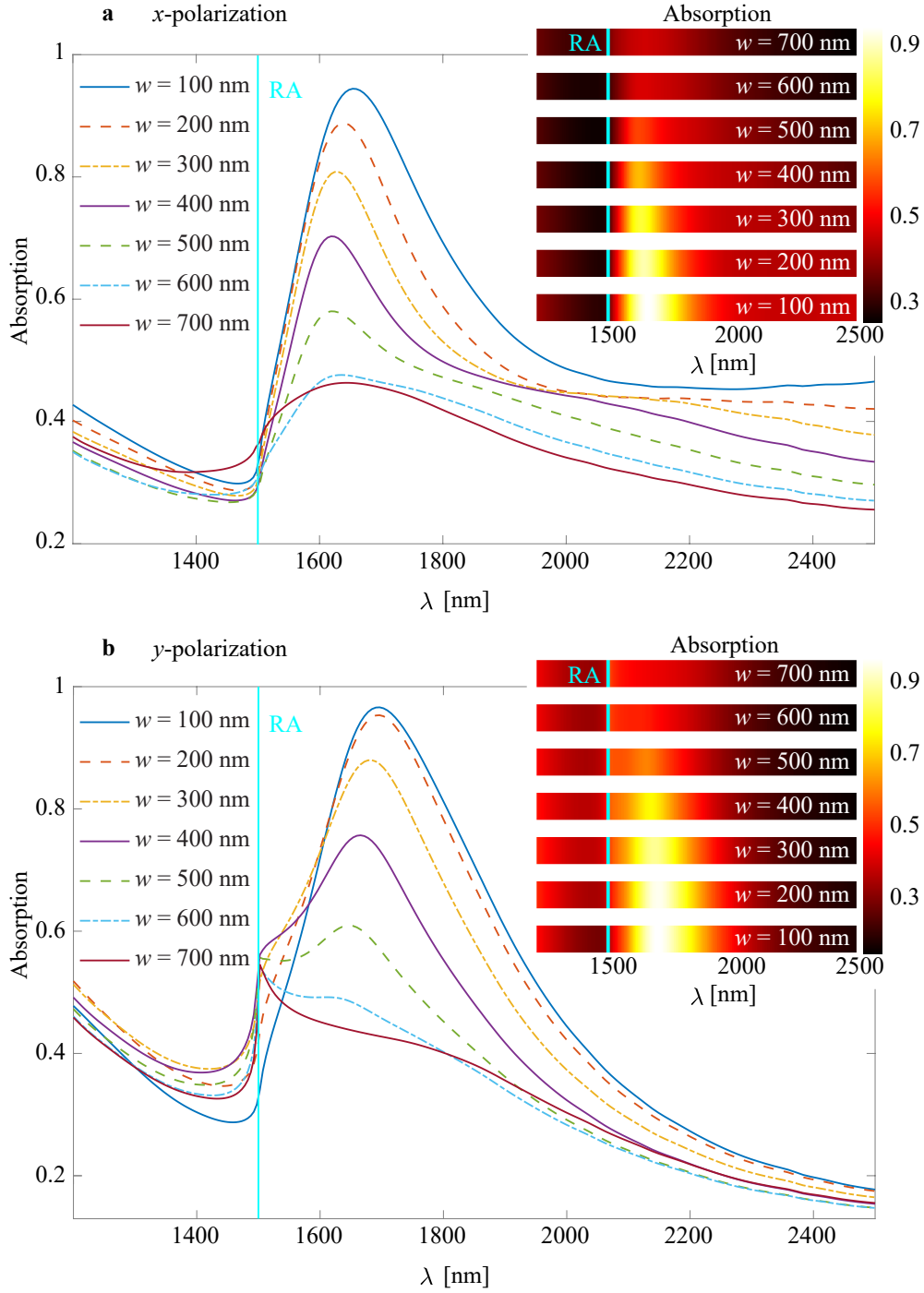
Figure S4: Resonant excitations in the interconnected MXene antennas arranged in the periodic array. Antennas in the uniform surrounding with $n = 1$. The absorption spectra are obtained with full-wave numerical simulations. We consider MXene antennas of cube shape with $a_x = a_y = a_z = 700$ nm connected with 'bridges' with the width of $w = 100$ nm to 700 nm by the step of 100 nm. **a** and **b** correspond to the illumination of light with x- or y-polarization respectively (see Figure 1**c**). The cuboids are placed in a periodic lattice with pitches $D_y = D_x = 1500$ nm. The solid cyan lines denote the Rayleigh anomaly wavelengths: 'RA' denotes the Rayleigh anomaly.
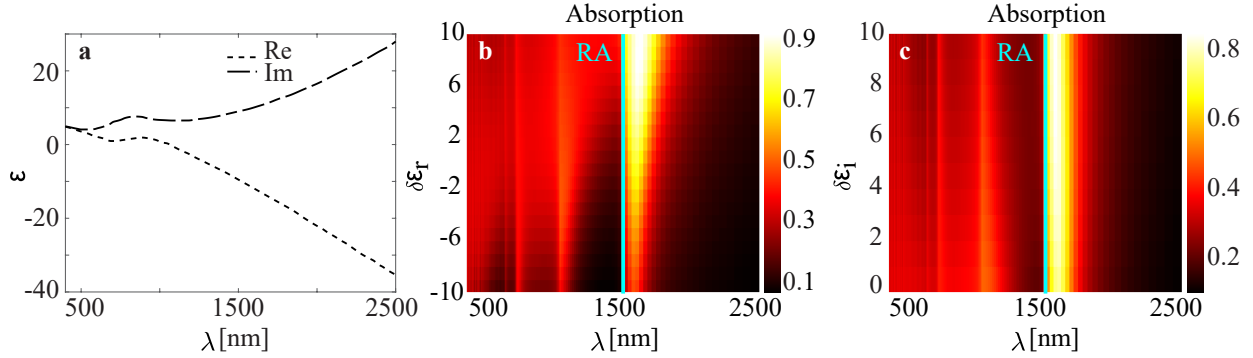
Figure S5: **a** Real and imaginary parts of $Ti_3C_2T_x$ permittivity (ε). The data points are taken from Ref. [1], and the film thickness is 400 nm. **b** and **c** Resonant response of the MXene sphere array depending on the variation of the permittivity. In panel **b**, the absorption is shown for the variation of the real part and the fixed imaginary part. In panel **c**, the absorption is shown for the variation of the imaginary part and the fixed real part. The radius is $R = 450$ nm, and the periodicities $D_x = D_y = 1500$ nm in both x- and y-directions. The antennas are surrounded by free space with $n = 1$. The solid cyan lines denote the Rayleigh anomaly wavelengths.
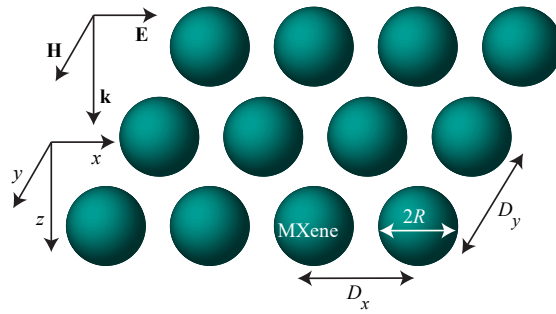

Figure S6: Sketch of the antenna lattice made of Ti3C2Tx MXene with the diameter $2R$. Antennas are placed in a homogeneous medium. For strong multipolar resonances and collective effects in this periodic arrangement, antennas are spaced with the distance of Dx and D_y in the x- and y-directions, respectively, and they are illuminated with the x-polarized light.
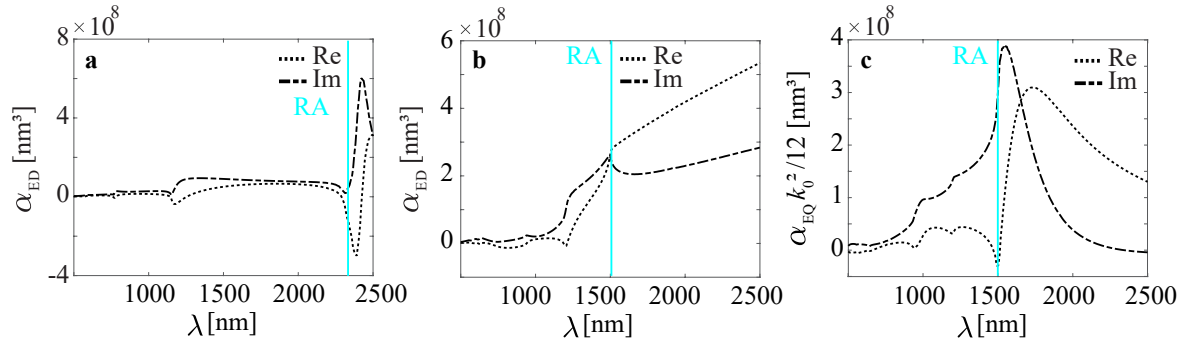
5

Figure S7: Real and imaginary parts of ED and EQ effective polarizability of sphere arrays. **a** ED effective polarizability of $R = 200$ nm with $D_x = 500$ nm and $D_y = 2300$ nm. ED and EQ effective polarizabilities of $R = 450$ nm with $D_x = 1500$ nm and $D_y = 1200$ nm in **b** and **c**, respectively. α_{EQ} is multiplied by $k_0^2/12$ in which k_0 is the wave number in free space. Cyan solid lines 'RA' denote the Rayleigh anomaly wavelengths.

References

[1] K. Chaudhuri, M. Alhabeb, Z. Wang, V. M. Shalaev, Y. Gogotsi, A. Boltasseva, *ACS Photonics* **2018**, *5*, 3 1115.
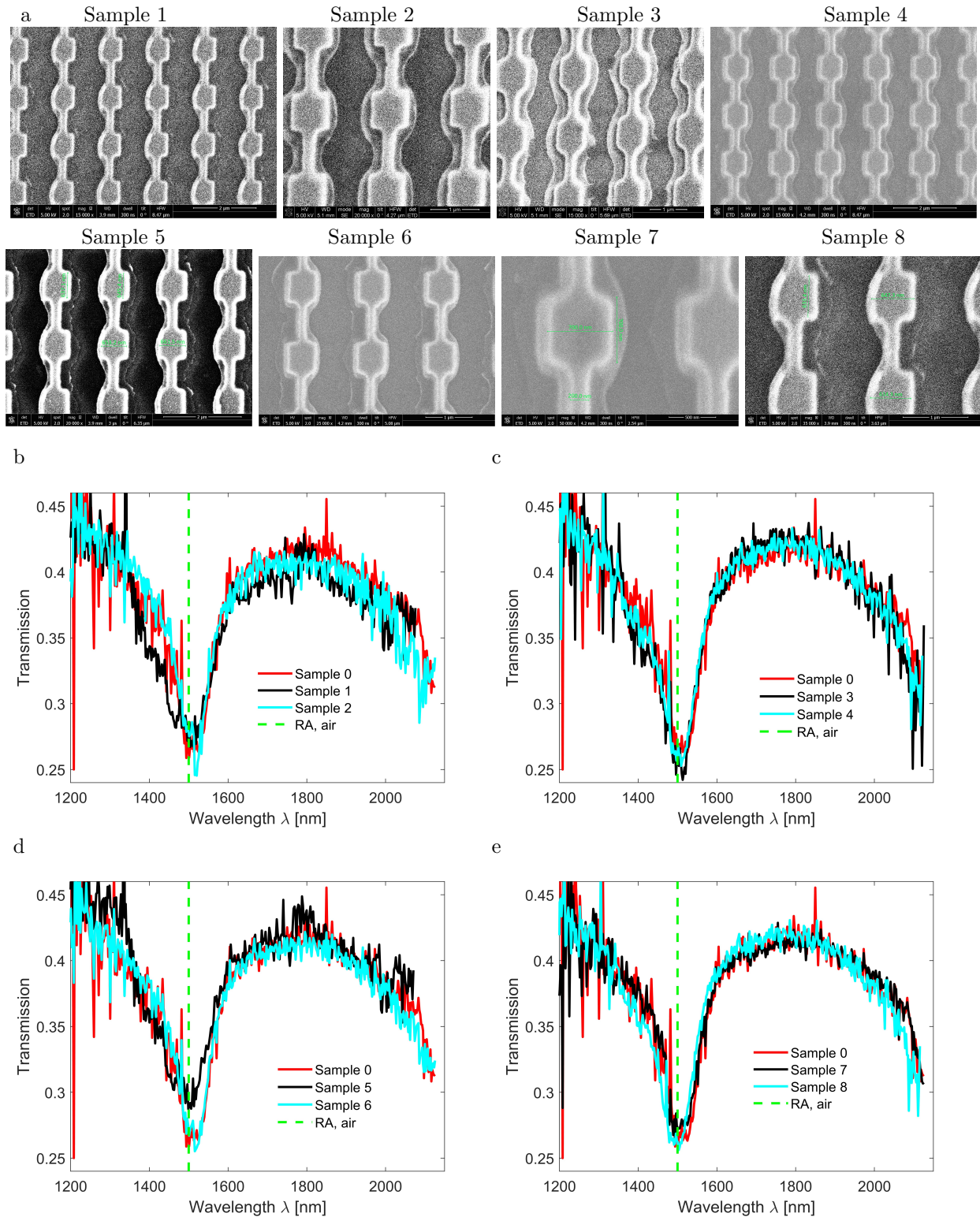
Figure S8: Repeatability of experimental measurements. **a** Scanning electron microscope images of several additional samples (#1 through #8) fabricated with the same procedure as reported in the main text. **b-e** Measurements of transmission corresponding to Samples #1 through #8. Results for Sample #0 are presented in the main text.